PFC/JA–89–25

Nonlinear Theory of Quasi–Optical Gyrotron with an Electron Beam at an Oblique Angle

Wang, C.Y., [1] Kreischer, K.E., Temkin, R.J.

Plasma Fusion Center

Massachusetts Institute of Technology

Cambridge, MA 02139

May 1989

This work was supported by U.S. DOE Contract DE–AC02–78ET51013.

[1] Visiting scientist from Zhenjiang University, P.R. China

May 1, 1989

Nonlinear Theory of Quasi-optical Gyrotron with an Electron Beam at an Oblique Angle

C.Y.Wang* K.E.Kreischer
R.J.Temkin
Massachusetts Institute of Technology
Plasma Fusion Center
Cambridge, MA 02139

In the quasi-optical gyrotron with a Fabry-Perot cavity one can inject the electron beam at an oblique angle with respect to the optical axis of the cavity. This angle has a great inflence on the gain mechanism, Doppler frequency shift and saturation length of interaction. Numerical simulations show that there exist two regimes of operation when the angle changes from zero to 90 degrees. When the angle is small (including zero degrees), one identifies the Doppler-shifted regime with small negative optimized detuning and small optimized E-field amplitude. When the angle is large (including 90 degrees), one identifies the gyrotron-like regime with large negative optimized detuning and large optimized E-field amplitude. The quasi- optical gyrotron is quite efficient for harmonic operation.

*visiting scientist from Zhejiang University, P.R. China

1. Introduction

One of the major efforts in gyrotron research is to reach high frequencies, at present, the submillimeter waveband. Compared with other free-electron devices, the gyrotron bears the merits of simplicity in structure for both the cavity and the magnetic field, low voltage and high efficiency. When operating at high frequencies, the mode density in the gyrotron becomes so large that a waveguide cavity will be difficult to use due to the problem of mode competition. It is natural to adopt the open cavity widely used in lasers as an alternative. Due to the small Fresnel number in millimeter and submillimeter wavelengths the cavity used in gyrotrons bears the name "quasi-optical".

There have been quite a few linear and nonlinear theories [1-10] published so far on the quasi-optical gyrotron. In these papers, geometries with the radiation beam parallel and perpendicular to the electron beam have been explored in great detail. The influence of an arbitrary angle between the radiation and electron beams was included in some theories[1-4,8,9] but hasn't been explored in full detail so far. Analysis shows that the injection angle has great inflence on gain mechanism, Doppler frequency shift and saturation length of interaction. In this paper the formulation in Ref.6 which was developed for a perpendicular injection geometry is extended to include geometries with arbitary injection angles. The influence of different angles on the efficiency for the second harmonic is also analyzed.

Two regimes of operation are identified when the angle changes from zero to 90 degrees. When the angle is small, the $k_{\|}v_{\|}$ term is significant in contributing to the Doppler shift of the frequency. This is the Doppler-shifted regime where the absolute value of the optimized detuning is smaller compared with that for the gyrotron-like regime. When the angle is large, the frequency is mainly decided by the cyclotron frequency of the electron. This is the gyrotron-like regime where the absolute value of the optimized detuning is relatively larger. The optimized efficiency for the gyrotron-like regime is usually higher than that for the Doppler-shifted regime.

The scheme with a tilted injection angle introduces a new degree of freedom to adjust the interaction length so that the efficiency can be optimized. This is a new feature of gyrotron operation. It may be easier to make the angle adjustable than to change the mirror spacing. Also it provides the

means to switch operation between Doppler-shifted and gyrotron emission within one device. If the angle is adjustable, one can tune the frequency mechanically without changing voltage or magnetic field.

This paper is organized as follows. Section 2 develops a linear theory for the field profile of the step function, different from Ref.1 in that it is a two-dimensional theory including the effect of harmonics. Section 3 derives the working nonlinear equations for the Gaussian field profile. Section 4 presents results from the nonlinear simulation and analysis. Section 5 gives the conclusions.

2. Linear Harmonic Theory

Choose coordinate frames as in Fig.1, where the primed frame is relative to the rf beam and the unprimed one to the electron beam. For simplicity the direction of the electric field is set to be perpendicular to the magnetic field which is in the z-axis. The y-axis lies in the plane decided by the magnetic field and the wave vector. Denoting the angle between the two beams as α, one obtains the following relations for transforming the two coordinates:

$$x' = x \tag{1}$$

$$y' = ycos\alpha + zsin\alpha \tag{2}$$

$$z' = -ysin\alpha + zcos\alpha \tag{3}$$

The fields in our linear model are chosen as plane standing waves so the mirrors in Fig.1 should be plane mirrors. The E and B fields can be expressed as

$$\mathbf{E} = \mathbf{e}'_{\mathbf{x}} E_0 cos\omega t sin(k_\perp y - k_\parallel z) \tag{4}$$

$$\mathbf{B} = \mathbf{e}'_{\mathbf{y}} E_0 sin\omega t cos(k_\perp y - k_\parallel z) \tag{5}$$

where $\mathbf{e}'_{\mathbf{x}} = \mathbf{e}_{\mathbf{x}}, \mathbf{e}'_{\mathbf{y}} = \mathbf{e}_{\mathbf{y}} cos\alpha + \mathbf{e}_{\mathbf{z}} sin\alpha$, $k_\perp = ksin\alpha$, $k_\parallel = kcos\alpha$. E_0 is the amplitude of the electric field, ω is the circular frequency and $k = \omega/c$ is the wave number of the plane wave.

Using standard plasma kinetic approach[11], the perturbed distribution function can be obtained:

$$f_1(\mathbf{p},\mathbf{r},t) = |e| \int_{-(l/2+z)/v_{\|}}^{0} d\tau(\mathbf{E} + \mathbf{v} \times \mathbf{B}/c) \cdot \frac{\partial f_0}{\partial \mathbf{p}} \tag{6}$$

where l is the interaction length and c is the light velocity, the origin of the frame is at the middle of l. $v_{\|}$ is the velocity component of the electron parallel to the d-c magnetic field. τ is the time variable on the unperturbed orbit. e is the electrical charge of the electron. The equilibrium distribution function f_0 is chosen in the calculation as monoenergetic:

$$f_0 = \frac{1}{2\pi p_{\perp}} \delta(p_{\perp} - p_{\perp 0})\delta(p_{\|} - p_{\|0}) \tag{7}$$

The interaction power per unit x-length is obtained from

$$P = \int \mathbf{J}_{\perp} \cdot \mathbf{E} dy dz \tag{8}$$

where the perturbed current $J_{\perp} = -2\pi|e|n_0 \int d^2 p v_{\perp} f_1$. n_0 is the number density of electrons.

Assuming the electron beam is symmetrical in y direction, which is often the case, and averaging P in a time interval containing an integer number of $2\pi/\omega$, one obtains

$$P = -\frac{\pi r_b n_0 |e|^2 E_0^2}{2m} \sum_n \int_{-\infty}^{\infty} dp_{\|} \int_0^{\infty} \frac{p_{\perp}^2}{\gamma} dp_{\perp} \int_0^{l} dz J_n'^2 \left(\frac{k_{\perp} v_{\perp}}{\omega_c}\right) \left[\left(\frac{sin\Omega_1 z/v_{\|}}{\Omega_1} + \frac{sin\Omega_2 z/v_{\|}}{\Omega_2}\right) \frac{\partial f_0}{\partial p_{\perp}} - \frac{cos\theta}{\gamma mc} \left(\frac{sin\Omega_1 z/v_{\|}}{\Omega_1} - \frac{sin\Omega_2 z/v_{\|}}{\Omega_2}\right) \left(p_{\perp} \frac{\partial f_0}{\partial p_{\|}} - p_{\|} \frac{\partial f_0}{\partial p_{\perp}}\right)\right] \tag{9}$$

where $\Omega_1 = \omega + k_{\|} v_{\|} - n\omega_c, \Omega_2 = \omega - k_{\|} v_{\|} - n\omega_c, \omega_c = \Omega/\gamma, \Omega = eB_0/mc$ is the nonrelativistic cyclotron frequency, B_0 is the d-c magnetic field, m is the electron rest mass, γ is the relativistic energy factor of the electron, r_b is the radius of the beam.

Substuting equation (7) into equation (9) and performing the manipulations with the artificial intelligence package MACSYMA on a VAX computer, one obtains

$$P = \frac{r_0 n_0 |e|^2 E_0^2 c^2}{4m\gamma v_\perp} \sum_n G_n \tag{10}$$

The gain function G_n is

$$G_n = G_E + G_B cos\alpha \tag{11}$$

where the contribution from the electric field is

$$\begin{aligned} G_E = J_n'\left(\frac{k_\perp v_\perp}{\omega_c}\right)\beta_\perp \Bigg\{ & J_n'\left(\frac{k_\perp v_\perp}{\omega_c}\right)\beta_\perp^2 kl \sum_{i=1}^{2} \frac{sin(\Omega_i l/v_\parallel)}{\Omega_i^2} \\ & + 2\beta_\parallel \left[J_n''\left(\frac{k_\perp v_\perp}{\omega_c}\right)\frac{k_\perp v_\perp}{\omega_c} + J_n'\left(\frac{k_\perp v_\perp}{\omega_c}\right)\right] \sum_{i=1}^{2} \frac{1 - cos(\Omega_i l/v_\parallel)}{\Omega_i^2} \\ & - 2J_n'\left(\frac{k_\perp v_\perp}{\omega_c}\right)\beta_\parallel \beta_\perp^2 \omega \sum_{i=1}^{2} \frac{1 - cos(\Omega_i l/v_\parallel)}{\Omega_i^3} \Bigg\} \end{aligned} \tag{12}$$

and the contribution from B field is

$$\begin{aligned} G_B = J_n'\left(\frac{k_\perp v_\perp}{\omega_c}\right)\beta_\perp \Bigg\{ & 2J_n'\left(\frac{k_\perp v_\perp}{\omega_c}\right)\beta_\parallel \beta_\perp^2 k_\parallel c \sum_{i=1}^{2} \frac{1 - cos(\Omega_i l/v_\parallel)}{\Omega_i^3} \\ & + J_n'\left(\frac{k_\perp v_\perp}{\omega_c}\right)\beta_\perp^2 l \frac{n\omega_c - \omega}{v_\parallel} \sum_{i=1}^{2} \frac{(-1)^i sin(\Omega_i l/v_\parallel)}{\Omega_i^2} \\ & - \left[J_n'\left(\frac{k_\perp v_\perp}{\omega_c}\right)(2\beta_\parallel^2 - \beta_\perp^2) + 2J_n''\left(\frac{k_\perp v_\perp}{\omega_c}\right)\frac{k_\perp v_\perp}{\omega_c}\beta_\parallel^2 \right] \sum_{i=1}^{2} \frac{(-1)^i [1 - cos(\Omega_i l/v_\parallel)]}{\Omega_i^2} \Bigg\} \end{aligned} \tag{13}$$

In the case of zero degrees and zero detuning (The detuning is defined in Eq.(38) and equal to $-\Omega_2 l/v_\parallel$ here), after dropping two small terms proprotional to Ω_1^{-1} and Ω_1^{-2} respectively, the criterion for gain is reduced to

$$\beta_{\perp 0}^2 > 2\beta_{\parallel 0}(1 - \beta_{\parallel 0}) \tag{14}$$

which agrees with Ref.6 where a traveling wave is assumed. At 90 degrees the backward component contributes considerably to the gain. The behavior of the gain function G_n with different injection angle α for the harmonics is

similar to that for the fundamental described in Ref.9. Note that there is no gain for the harmonics at zero degrees because $k_\perp = 0$ and the electron sees constant E field on the wave front.

3. Nonlinear Equations for Particles

A Gaussian field profile is assumed for the nonlinear simulation. The E-field amplitude in Eqs.(4) and (5) now takes the form

$$E(y', z') = E_0 exp\{-(x'^2 + y'^2)/[r_0^2(1 + z'^2/z_R^2)^2]\}/(1 + z'^2/z_R^2) \qquad (15)$$

where x', y' and z' are given in Eqs.(1) to (3), $r_0 = \sqrt{\lambda L/\pi}$ is the spot size and $z_R = r_0^2\omega/2c$ is the Rayleigh length. Normally $z_R \gg z$. Noting that for an electron beam the tranverse dimension is much smaller than the longitudinal dimension, one has $x, y \ll z$ and $y' \approx z sin\alpha$. The approximation

$$E(z) = E_0 exp(-z^2 sin^2\alpha/r_0^2) \qquad (16)$$

is used throughout the rest of this paper. The independent variables are $p_\perp, \psi$, (transverse momentum and angle) x_g and y_g (guiding center coordinates), which are related to the transverse momenta and coordinates p_x, p_y, x and y by

$$p_x = p_\perp cos\psi \qquad (17)$$
$$p_y = p_\perp sin\psi \qquad (18)$$
$$y_g = y + p_x/m\Omega \qquad (19)$$
$$x_g = x - p_y/m\Omega \qquad (20)$$

The equations of motion then reduce to

$$dp_\perp/dz = (-em\gamma/p_z)cos\psi E + (ecos\alpha/c)cos\psi B \qquad (21)$$

$$d\psi/dz = m\Omega/p_z + eBsin\alpha/cp_z + m\gamma esin\psi E/p_\perp p_z - eBcos\alpha sin\psi/cp_\perp \qquad (22)$$

$$dy_g/dz = (-e\gamma/p_z\Omega)[E + B(p_\perp sin\psi sin\alpha - p_z cos\alpha)/\gamma mc] \qquad (23)$$

$$dp_z/dz = -(ep_\perp/cp_z)Bcos\psi cos\alpha \qquad (24)$$

$$dx_g/dz = -(p_\perp sin\alpha/p_z B_0)Bcos\psi \qquad (25)$$

Because the x-dependence which causes only high order effects in Eq.(15) is neglected in this paper, x_g is treated as constant and Eq.(25) is not used.

In the following derivations we have used the identities

$$sink_\perp y = sink_\perp y_g[J_0(Q) + 2\sum_{l=1}^{\infty}(-1)^l J_{2l}(Q)cos2l\psi] - 2cosk_\perp y_g \sum_{l=0}^{\infty}(-1)^l J_{2l+1}(Q)cos(2l+1)\psi \qquad (26)$$

$$cosk_\perp y = cosk_\perp y_g[J_0(Q) + 2\sum_{l=1}^{\infty}(-1)^l J_{2l}(Q)cos2l\psi] + 2sink_\perp y_g \sum_{l=0}^{\infty}(-1)^l J_{2l+1}(Q)cos(2l+1)\psi \qquad (27)$$

where $Q = k_\perp p_\perp/m\Omega$. Since to the lowest order $d\psi/dt \simeq \Omega/\gamma$ and $\omega \simeq n\Omega/\gamma$, only terms with $cosn\psi$ are retained in Eqs.(21) to (24). Neglecting the rapidly varying terms yields

$$\frac{dp_\perp}{dz} = -\frac{em\gamma}{p_z}E(z)J_n'(Q)cos(\omega t - n\psi)cos(k_\perp y_g - k_\parallel z - n\pi/2) - \frac{ecos\alpha}{c}E(z)J_n'(Q)sin(\omega t - n\psi)sin(k_\perp y_g - k_\parallel z - n\pi/2) \qquad (28)$$

$$\frac{dp_z}{dz} = \frac{ep_\perp cos\alpha}{cp_z}E(z)J_n'(Q)sin(\omega t - n\psi)sin(k_\perp y_g - k_\parallel z - n\pi/2) \qquad (29)$$

$$\frac{d\psi}{dz} = \frac{m\omega}{p_z} - \frac{eE(z)m\gamma}{p_z p_\perp}\frac{nJ_n(Q)}{Q}\left(1 - \frac{p_\perp sin\alpha}{m\gamma c}\frac{Q}{n}\right) sin(\omega t - n\psi)cos(k_\perp y_g - k_\parallel z - n\pi/2) + \frac{eE(z)cos\alpha}{cp_\perp}\frac{nJ_n(Q)}{Q}cos(\omega t - n\psi)sin(k_\perp y_g - k_\parallel z - n\pi/2) \quad (30)$$

$$\frac{dy_g}{dz} = \frac{e\gamma E(z)}{p_z\Omega}J_n(Q)\left[\left(\frac{np_\perp sin\alpha}{\gamma mcQ} - 1\right) cos(\omega t - n\psi)sin(k_\perp y_g - k_\parallel z - n\pi/2) + \frac{p_z cos\alpha}{\gamma mc} sin(\omega t - n\psi)cos(k_\perp y_g - k_\parallel z - n\pi/2)\right] \quad (31)$$

where J_n is the Bessel function of order n. When $\alpha = 90^0$, these equations reduce exactly to Eqs.(10) to (12) in Ref.6.

4. Calculation And Analysis

A confocal cavity is assumed for the calculation model shown in Fig.1. With this practical model one should note that for fixed mirror radius the interaction length increases when the injection angle decreases. This model causes the optimized efficiency to be reached at a smaller E-field amplitude for small angles because of the longer interaction length. The angle where the electron beam just hits the edge of the mirror is defined as

$$\alpha_0 = arctan\left(\frac{2r_w}{L}\right) \quad (32)$$

where L is the mirror spacing and $r_w = r_0(1 + (L/z_R)^2/4)$ is the spot size on the mirror. The normalization length is defined as

$$L_0 = \begin{cases} L/cos\alpha & \text{if } \alpha \le \alpha_0 \\ r/sin\alpha & \text{if } \alpha \ge \alpha_0 \end{cases} \quad (33)$$

where $r = ((z_R tan\alpha)^2/r_0 - z_R tan\alpha\sqrt{(z_R tan\alpha/r_0)^2 - 4})/2$ is the spot size at the angle α. At angles less than α_0, the electron beam passes through the mirror. In practice, this can be achieved for a pencil beam by making a small hole in the mirror which has an insignificant effect on the rf field.

Set normalized interaction length $\zeta = z/L_0$, normalized electric field amplitude $\varepsilon = eE_0/mc^2$, normalized transverse and longitudinal momenta $u_\perp = p_\perp/mc, u_\parallel = p_z/mc, \theta = n\psi - \omega t, q = r_0\omega/tan\alpha c$, and $Y_g = k_\perp y_g$. Noting that $\gamma = \sqrt{1+u_\perp^2+u_\parallel^2}$, we obtain the following working equations:

$$\frac{du_\perp}{d\zeta} = L_0\varepsilon exp(-(L_0 sin\alpha\zeta/r_0)^2)J_n'(sin\alpha\omega u_\perp/\Omega)\left[cos\alpha sin\theta sin(Y_g - q\zeta - n\pi/2) - \frac{\gamma cos\theta cos(Y_g - q\zeta - n\pi/2)}{u_\parallel}\right] \quad (34)$$

$$\frac{du_\parallel}{d\zeta} = -L_0\varepsilon exp(-(L_0 sin\alpha\zeta/r_0)^2)J_n'(sin\alpha\omega u_\perp/\Omega)u_\perp/u_\parallel cos\alpha sin\theta sin(Y_g - q\zeta - n\pi/2) \quad (35)$$

$$\frac{d\theta}{d\zeta} = \frac{L_0}{cu_\parallel}(n\Omega - \gamma\omega) + L_0 n\varepsilon exp(-(L_0 sin\alpha\zeta/r_0)^2)J_n(sin\alpha\omega u_\perp/\Omega)\left[\left(\frac{n\Omega\gamma}{sin\alpha\omega u_\perp^2} - sin\alpha\right)\frac{sin\theta cos(Y_g - q\zeta - n\pi/2)}{u_\parallel} + \frac{n\Omega cos\alpha cos\theta sin(Y_g - q\zeta - n\pi/2)}{sin\alpha\omega u_\perp^2}\right] \quad (36)$$

$$\frac{dY_g}{d\zeta} = \frac{L_0\varepsilon sin\alpha\omega}{u_\parallel\Omega}exp(-(L_0 sin\alpha\zeta/r_0)^2)J_n(sin\alpha\omega u_\perp/\Omega)\left[\left(\frac{n\Omega}{\omega} - \gamma\right) cos\theta sin(Y_g - q\zeta - n\pi/2) - u_\parallel cos\alpha sin\theta cos(Y_g - q\zeta - n\pi/2)\right] \quad (37)$$

Eq. (37) is sometimes dropped since y_g doesn't change much during the traversal of the beam.

As a check of the validity of the nonlinear theory, the linear regime is examined first. After dropping the exponential factors (since the linear theory assumes a step-function field profile), Eqs.(34) to (37) were solved under small E-field amplitude and an average of Y_g over 0 to 2π was taken since in the linear theory there is no explicit relevance to the guiding center. Plotting efficiency versus detuning ξ at various angles one can get nearly the same curves as those produced from Eq.(11). The detuning is defined in Ref.(9) as

$$\xi = l(\omega_c - \omega + k_{\|} v_z)/v_z \tag{38}$$

These curves are very close to those in Ref.9 so that they are not shown here.

In Fig.2 one plots efficiency versus detuning ξ in the nonlinear regime for a pencil beam with no velocity spread and with $n = 1, U = 80kv, f = 140GHz, L = 5cm, p_\perp/p_{\|} = 1.93$. For comparison the curves for the corresponding linear cases are also shown in the graphs. One can see the detuning spectrum distorted from the linear case. Fig.2a is the case for the Doppler-shifted regime with $\alpha = 0^0$ and $\epsilon = 0.08$. By adjusting beam pitch angle or $p_\perp/p_{\|}$, efficiency would peak at the center, i.e. the optimized detuning for the Doppler-shifted regime is always small. If the beam pitch angle is too small, the maximum linear efficiency would be reached at $\xi = 7.5$. This is not a good operating state becaused of the low nonlinear efficiency. Fig.2b is the case for the gyrotron-like regime with $\alpha = 78^0$ and $\epsilon = 0.66$. One can see that the spectrum is nearly anti-symmetrical, which is characteristic of the gyrotron. Both cases have been optimized with respect to the E-field amplitude. The reason for smaller optimized E-field for the Doppler-shifted regime is the longer interaction length.

In Fig.3 one plots efficiency versus different angles at fixed detuning and E-field amplitude. Fig.3a is for the Doppler-shifted regime with $\xi = -0.5$ and $\epsilon = 0.08$. These two parameters are optimized for $\alpha = 0^0$. Fig.3b is for the gyrotron-like regime with $\xi = -11.0$ and $\epsilon = 0.66$ which are optimized for $\alpha = 81^0$. One can see clearly that there exist two distinct regimes of operation separated at $\alpha = 15^0$ in this group of parameters. Fig.3c is for the gyrotron-like regime for the second harmonic with $\xi = -12.5$. One can see that for higher harmonic the maximum efficiency is reached at higher optimized E-field, in our case $\epsilon = 1.85$. There is no graph of the second harmonic for the Doppler- shifted regime. That regime is not suitable for operation at harmonics since when α is small, the electron sees little variations in field amplitude in its cyclotron orbit.

Fig.4 gives efficiency optimized with respect to detuning versus various angles for the same parameters as in Fig.3a and 3b. Calculation shows that in the Doppler-shifted regime the optimum detuning ranges from -0.5 to -2.5 in our case. In the gyrotron-like regime the optimum detuning ranges from -7.5 to -14.5 in our case. One can see from Fig.4 that in the gyrotron regime, the maximum is not reached at 90^0, but at a smaller angle. This arises because

the interaction length at 90^0 is too short. By adjusting the mirror spacing L which relates the minimum spot size through $r_0 = \sqrt{\lambda L/\pi}$, one can shift the peak towards 90^0. This can also be accomplished by changing the injection angle. Fig.5a and 5b present efficiency versus normalized E-field amplitude for the two regimes.

High efficiency can also be achieved with high beam voltage. Fig.6 shows there is a wide range for tuning operation frequency or d-c magnetic field by changing the beam injection angle. Fig.6a plots optimized efficiency versus angle for $U = 450kv, p_\perp/p_\| = 1.0, f = 280GHz, n = 2, L = 20cm$ and $\epsilon = 2.4$. Fig.6b presents d-c magnetic field versus various angles.

In the following table are listed the parameters for two possible experiments for the second harmonic.

Possible Experiments

U(kV)	80	450
n	2	2
$\eta(\%)$	40.6	31.0
f(GHz)	280	280
B(T)	4.7	3.8
θ(deg.)	45	16
α	1.93	1.0
L/λ	23	93
E_{max}(kV/cm)	533	692

5. Conclusion

The linear and nonlinear theory of the quasi-optical gyrotron with the tilted beam-radiation geometry are presented in this paper. Analysis shows there exist two distinct regimes of operation. One is the Doppler-shifted regime with the angle ranging from zero to over 10 degrees depending on the parameters. The optimized absolute detuning and E-field amplitude are both small in this regime. The other is the gyrotron-like regime with the angle ranging from tens of degrees to 90 degrees. The optimized absolute detuning and E-field amplitude are both large compared with the Doppler-shifted regime. The scheme with a tilted angle provides an additional means

to adjust the interaction length to optimize the efficiency and to tune the frequency mechanically.

6. Acknowledgement

The authors appreciate helpful discussions with Dr.J.S.Wurtele and K.D.Pendergast. This research was conducted under U.S.D.O.E. contract DE-AC02-78ET-51013.

References

[1] K.E.Kreischer and R.J.Temkin, in *Infrared and Millimeter Waves*, Vol.7, New York: Academic Press, 1983, ch.8, p.418

[2] B.Levush, A.Bondeson, W.M.Manheimer and E.Ott, Int.J.Electronics, Vol.54,No.6,749(1983)

[3] S.Liu, Acta Electron., Vol.12, No.1, p.12(1984)

[4] V.L.Bratman, N.S.Ginzburg, G.S.Nusinovich, M.I.Petelin and P.S. Strelkov, Int.J.Electronics, Vol.51,No.4,541(1981)

[5] J.L.Vomvoridis, Int.J.IR/MM Waves, Vol.3,No.5,685(1982)

[6] J.L.Vormvoridis, P.Sprangle and W.M.Manheimer, in *Infrared and Millimeter Waves*, Vol.7, New York: Academic Press, 1983, ch.9, p.487

[7] A.Bondeson, W.M.Manheimer and E.Ott, in *Infrared and Millimeter Waves*, Vol.9, New York: Academic Press, 1983, ch.7, p.309

[8] S.Riyopoulos, C.M.Tang, P.Sprangle and B.Levush, Phys. Fluids,31(4), 924(1988)

[9] C.Wang, K.Kreischer and R.Temkin, IEEE Trans. Electron Devices, Vol.35,No.7,1166(1988)

[10] S.K.Ride and W.B.Colson, Appl.Phys., Vol.20, p.941(1979)

[11] N.A.Krall and A.W.Trivelpiece, *Principles of Plasma Physics*, McGraw-Hill Book Co., 403(1973)

Figure Captions

- Fig.1 Schematic for linear theory. Note that in the nonlinear theory a confocal cavity is assumed and the radiation bears a Gaussian profile. The primed frame is relative to the rf beam and the unprimed to the electron beam. Both x-axes point out of the paper.

- Fig.2a Efficiency is plotted versus detuning ξ at $\alpha = 0.0001^0$ for a 80-kV electron beam, $p_\perp/p_\parallel = 1.93, f = 140GHz, n = 1$ and $L = 5cm$. The upper graph is in the nonlinear regime with $\varepsilon = 0.08$. The lower one in the linear regime with $\varepsilon = 0.00025$.

- Fig.2b Efficiency versus detuning at $\alpha = 78^0$ for the same parameters as Fig.2a. In the upper graph $\varepsilon = 0.66$.

- Fig.3 Efficiency versus angles at fixed detuning and E-field amplitude for the same parameters as Fig.2a. Fig.3a is for the Doppler-shifted regime with $\xi = -0.5$ and $\varepsilon = 0.08$. Fig.3b is for the gyrotron-like regime with $\xi = -11.0$ and $\varepsilon = 0.66$. Fig.3c is for the gyrotron regime for the second harmonic with $\xi = -12.5$ and $\varepsilon = 1.85$.

- Fig.4 Efficiency optimized over detuning versus angles for the same parameters as Fig.3a and 3b. The solid line is for the Doppler-shifted regime with $\varepsilon = 0.08$ and the dash line for the gyrotron- like regime with $\varepsilon = 0.66$.

- Fig.5 Efficiency versus normalized E-field amplitude for the same parameters as Fig.2a. Fig.5a is for the Doppler-shifted regime and Fig.5b is for the gyrotron-like regime.

- Fig.6 Performance at high beam voltages. Fig.6a shows optimized efficiency versus angles for a 450-kV electron beam with $p_\perp/p_\parallel = 1.0, f = 280GHz, n = 2, L = 20cm$ and $\varepsilon = 2.4$. Fig.6b presents d-c magnetic field versus angles.

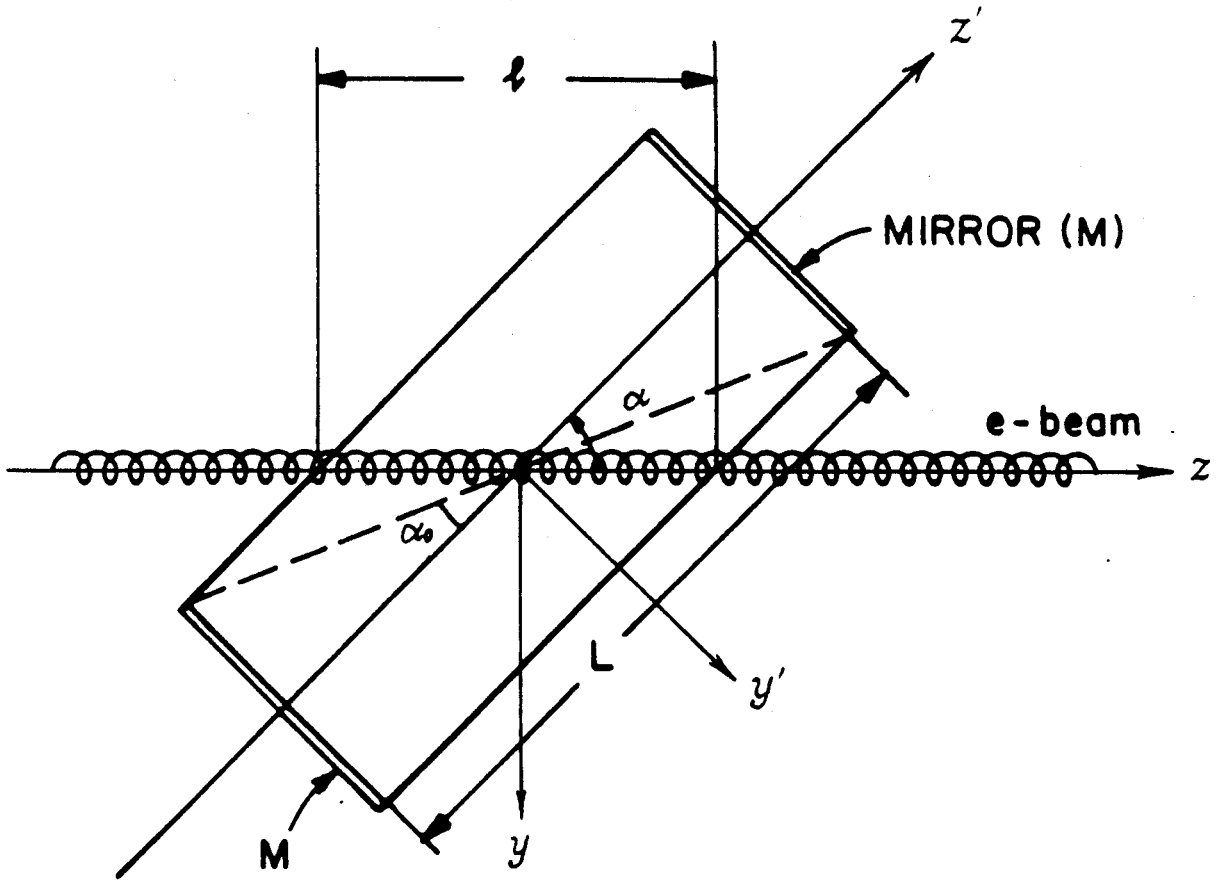

Fig. 1

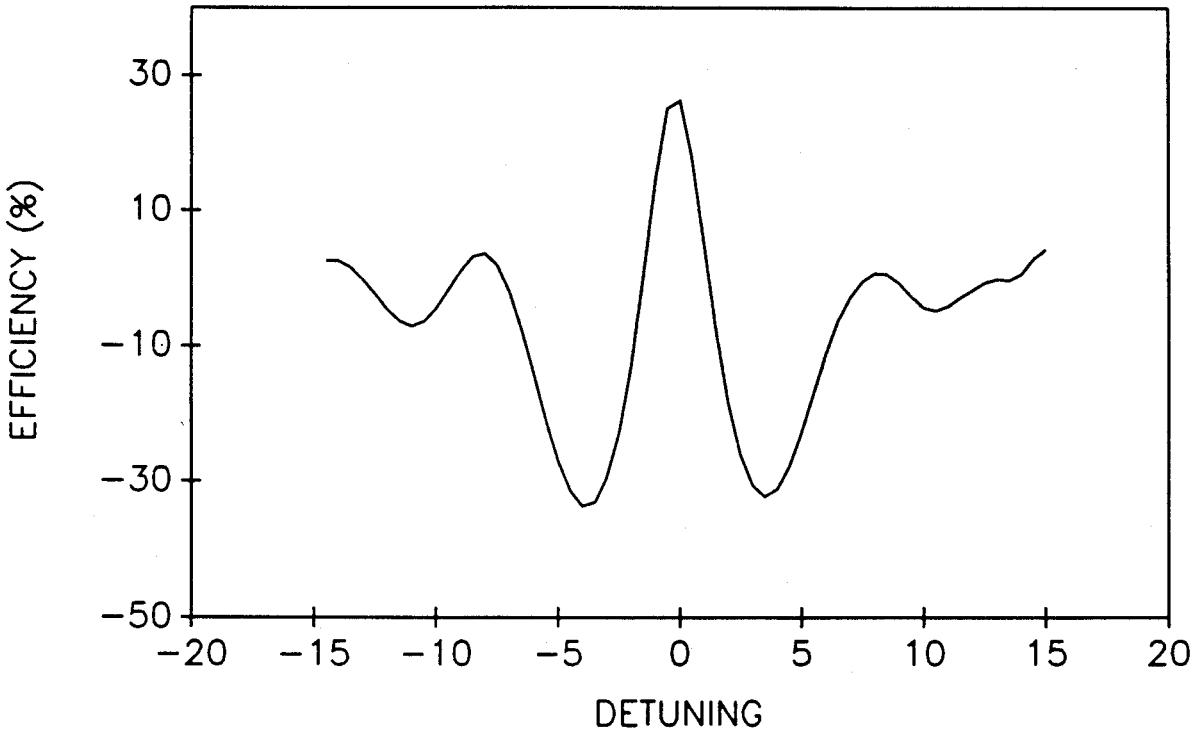
30
10
-10
-30
-50
EFFICIENCY (%)
-20
-15
-10
-5
0
5
10
15
20
DETUNING

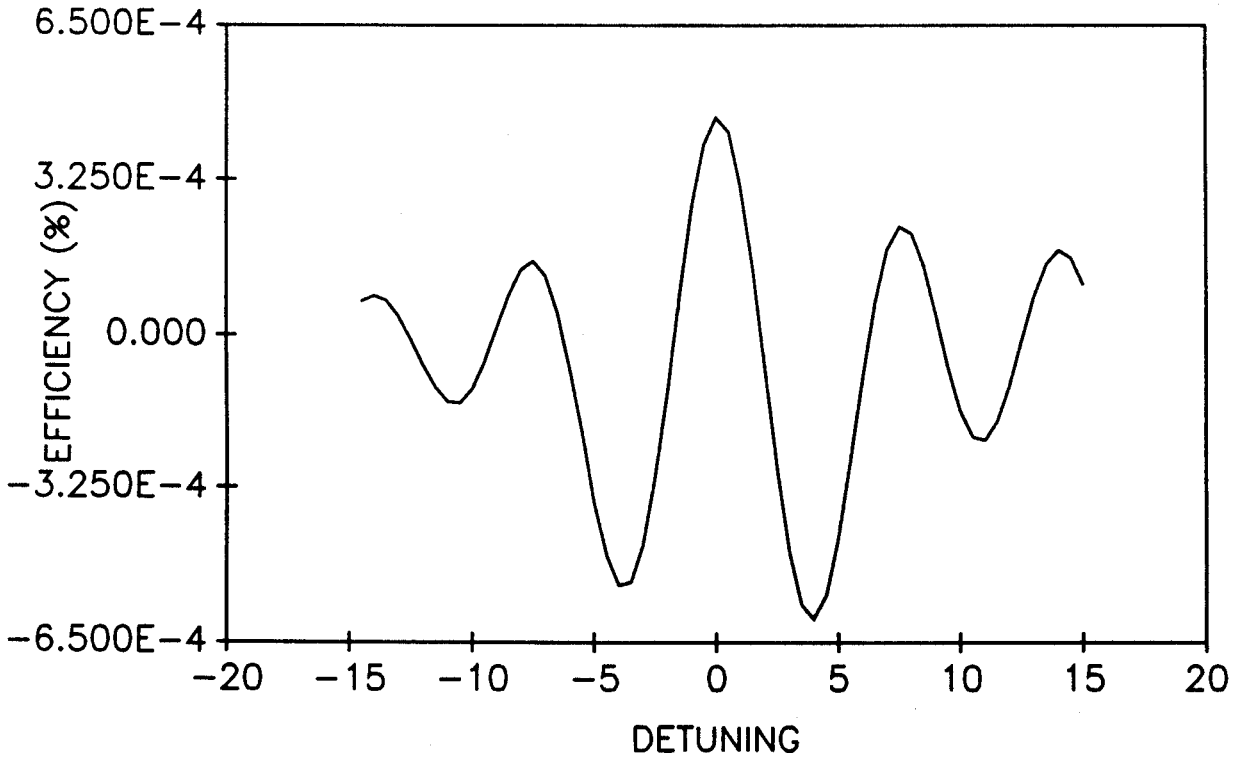
6.500E-4
3.250E-4
0.000
-3.250E-4
-6.500E-4
EFFICIENCY (%)
-20
-15
-10
-5
0
5
10
15
20
DETUNING

Fig. 2a

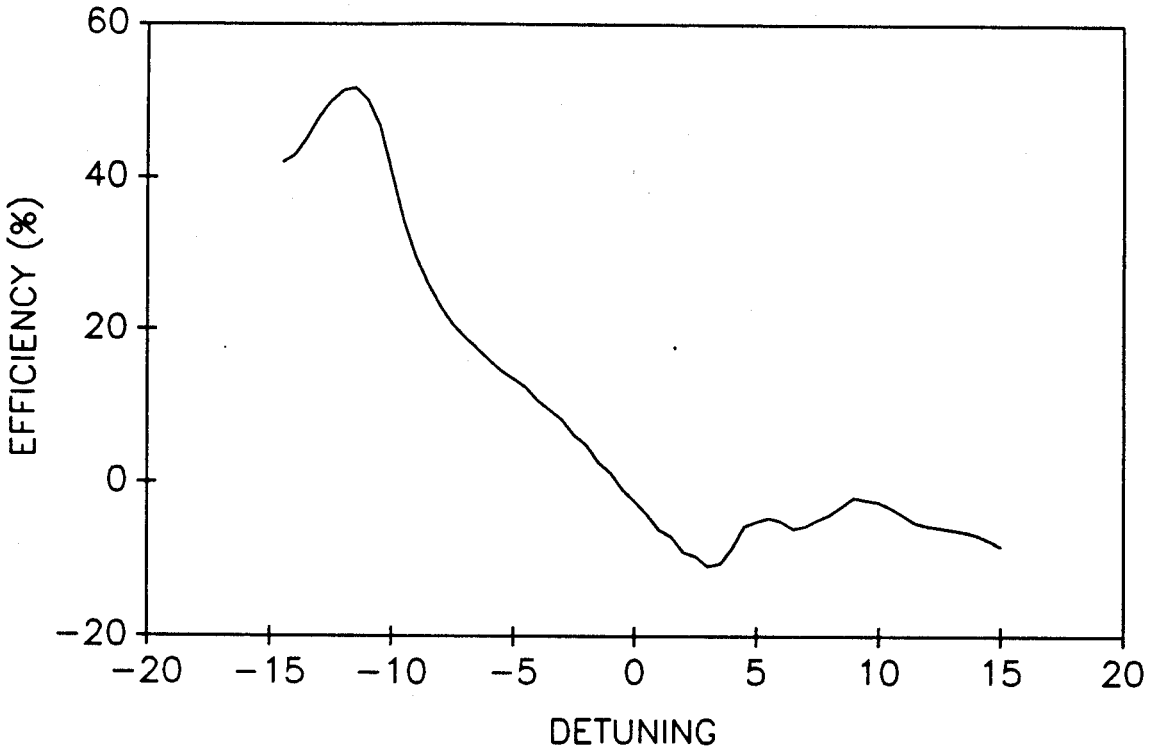
60
40
20
0
-20
EFFICIENCY (%)
-20
-15
-10
-5
0
5
10
15
20
DETUNING

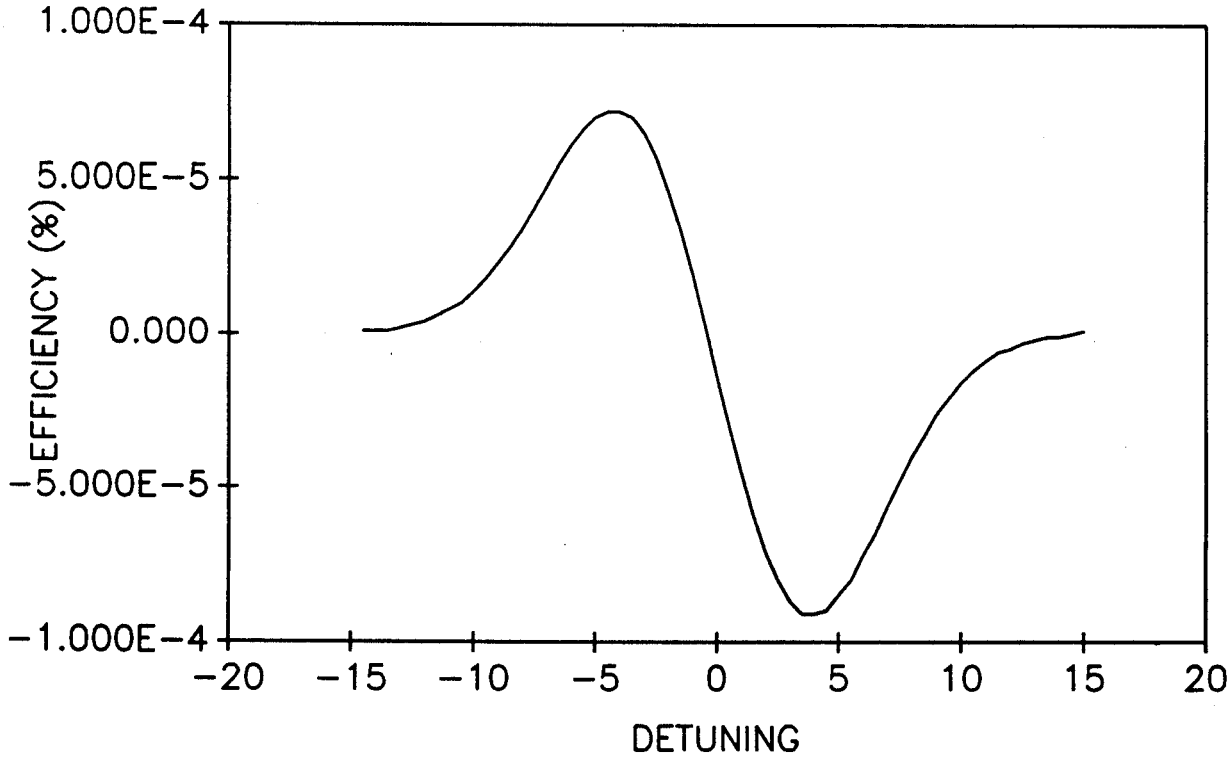
1.000E-4
5.000E-5
0.000
-5.000E-5
-1.000E-4
EFFICIENCY (%)
-20
-15
-10
-5
0
5
10
15
20
DETUNING

Fig. 2b

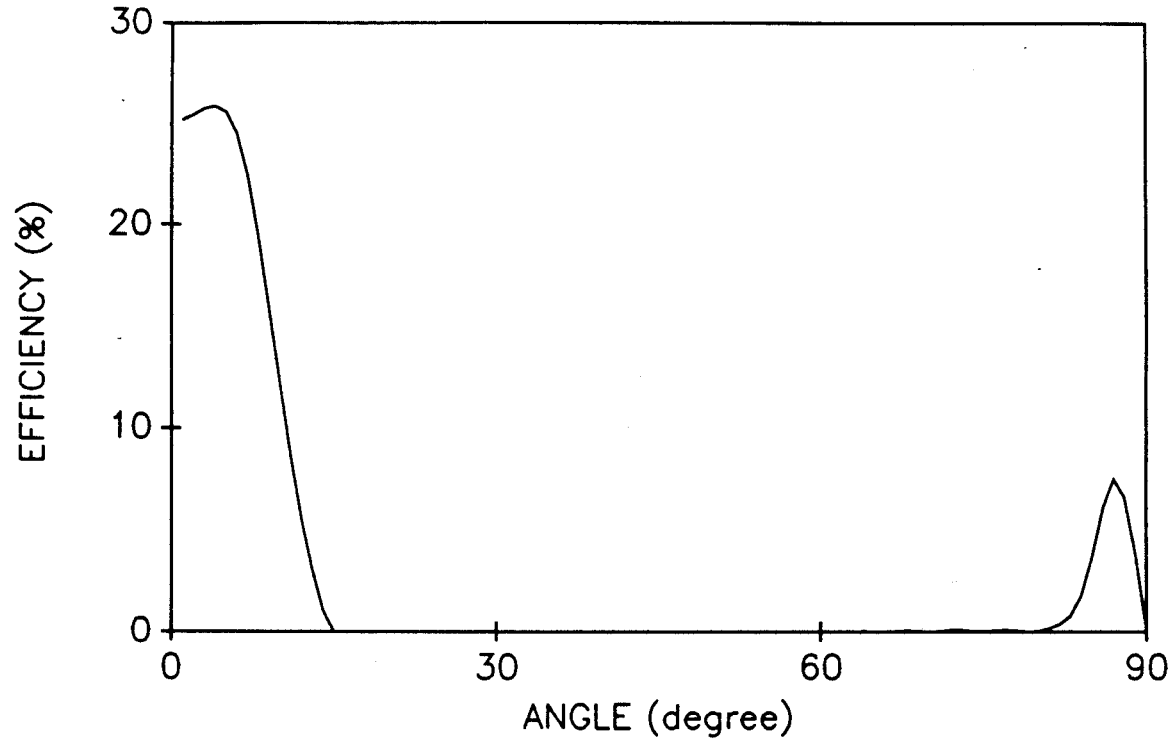
30
20
10
0
EFFICIENCY (%)
0
30
60
90
ANGLE (degree)

Fig. 3a

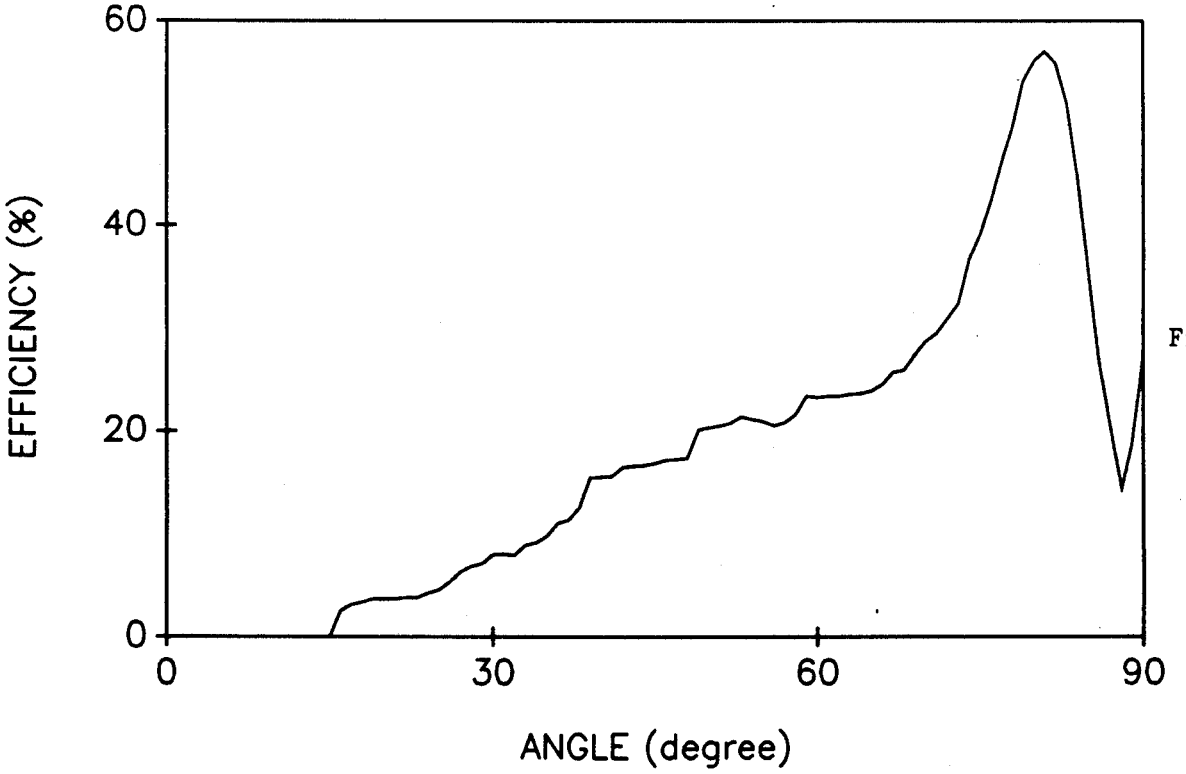
60
40
20
0
EFFICIENCY (%)
0
30
60
90
ANGLE (degree)

Fig. 3b

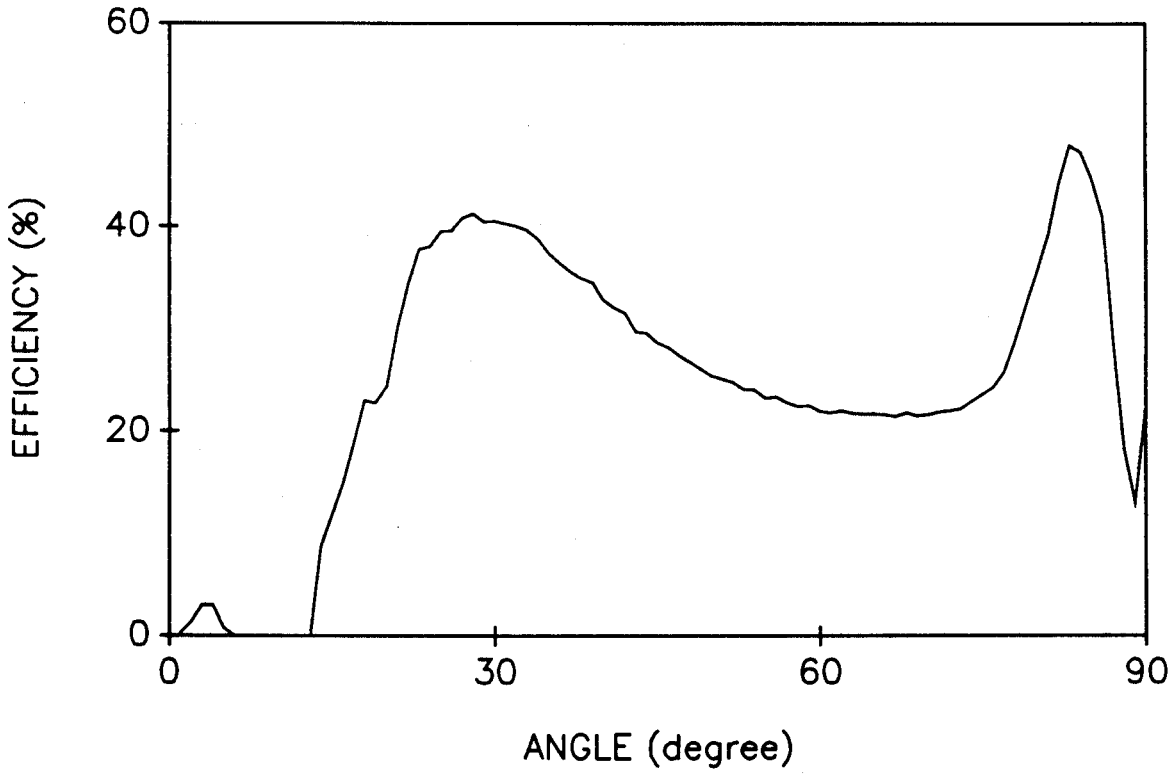

Fig. 3c

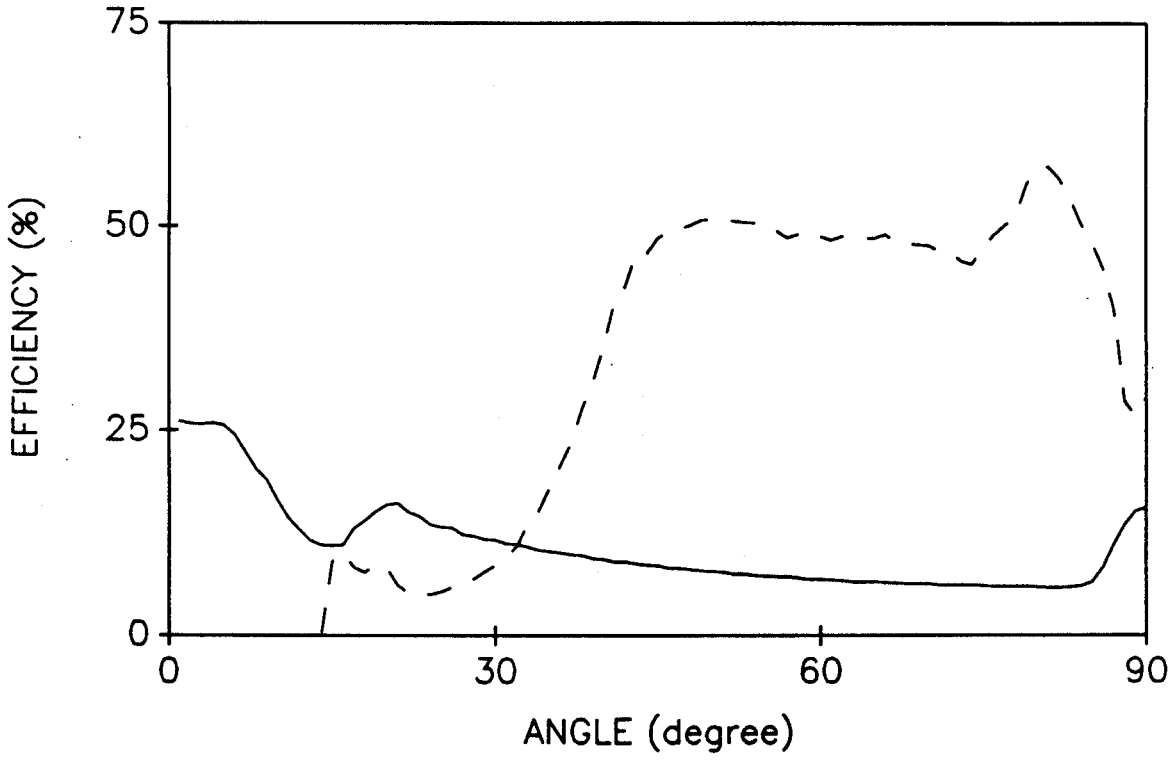

Fig. 4

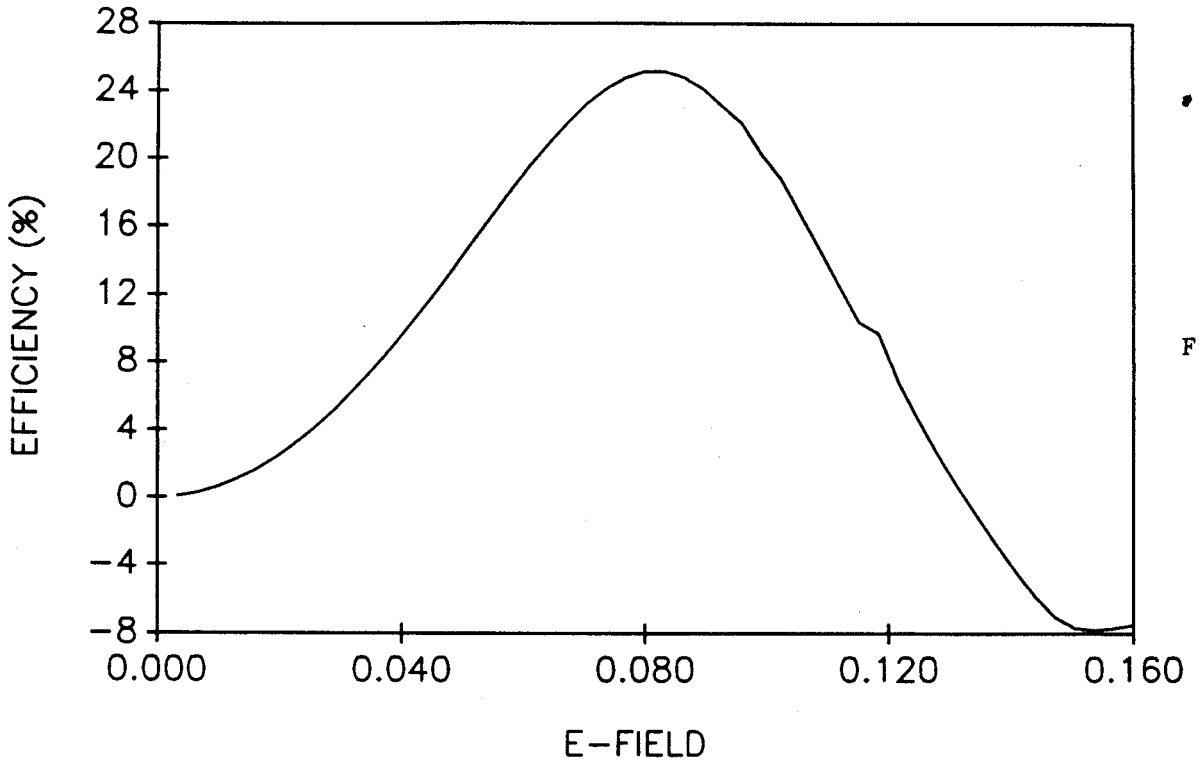
28
24
20
16
12
8
4
0
-4
-8
EFFICIENCY (%)
0.000
0.040
0.080
0.120
0.160
E-FIELD

Fig. 5a

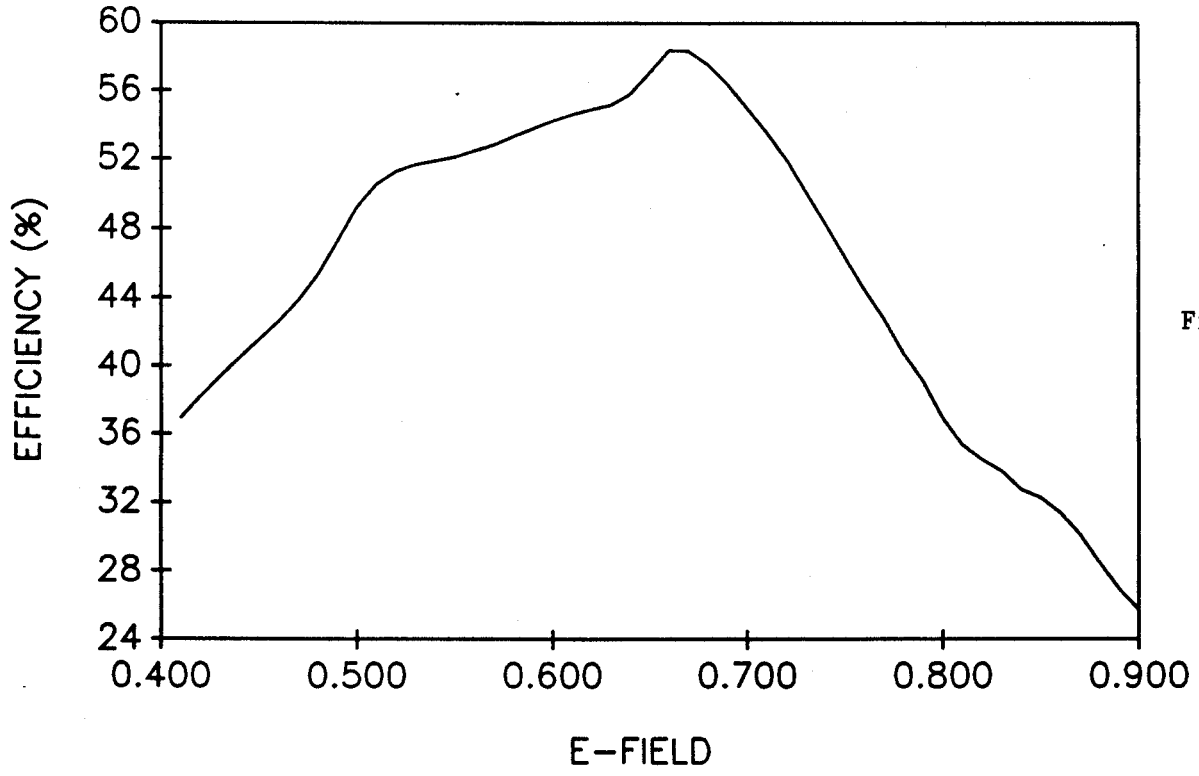
60
56
52
48
44
40
36
32
28
24
EFFICIENCY (%)
0.400
0.500
0.600
0.700
0.800
0.900
E-FIELD

Fig. 5b

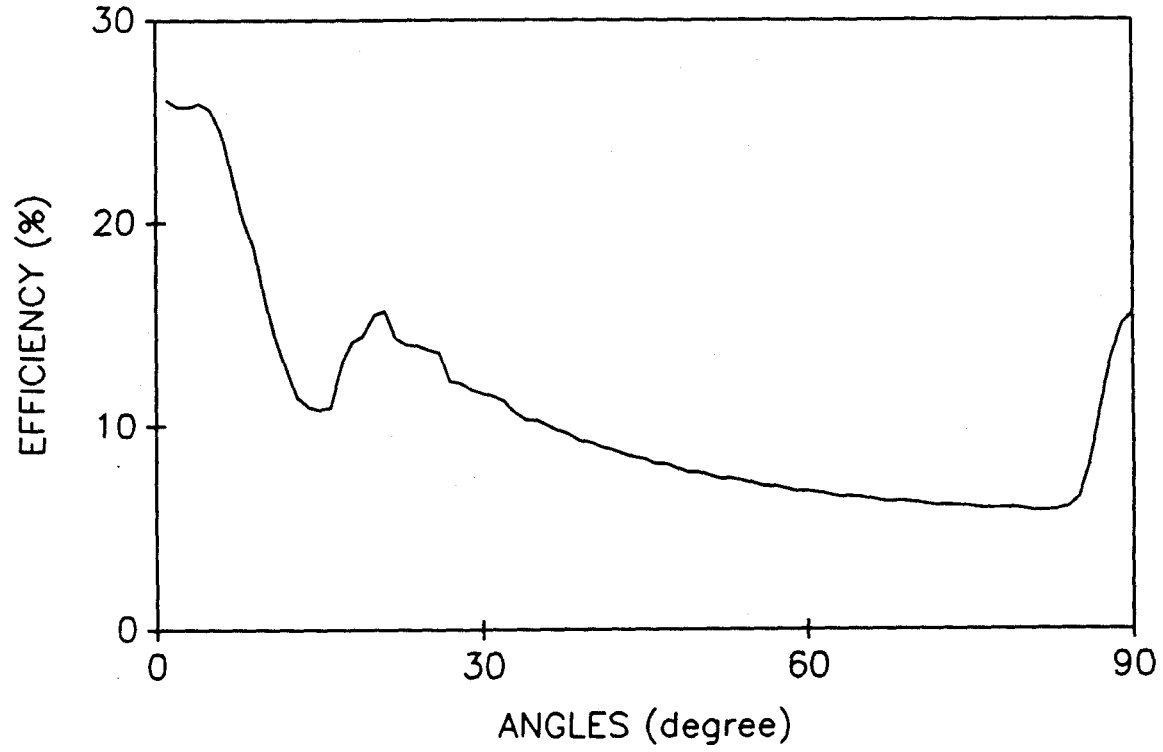
30
20
10
0
EFFICIENCY (%)
0
30
60
90
ANGLES (degree)

Fig.6a

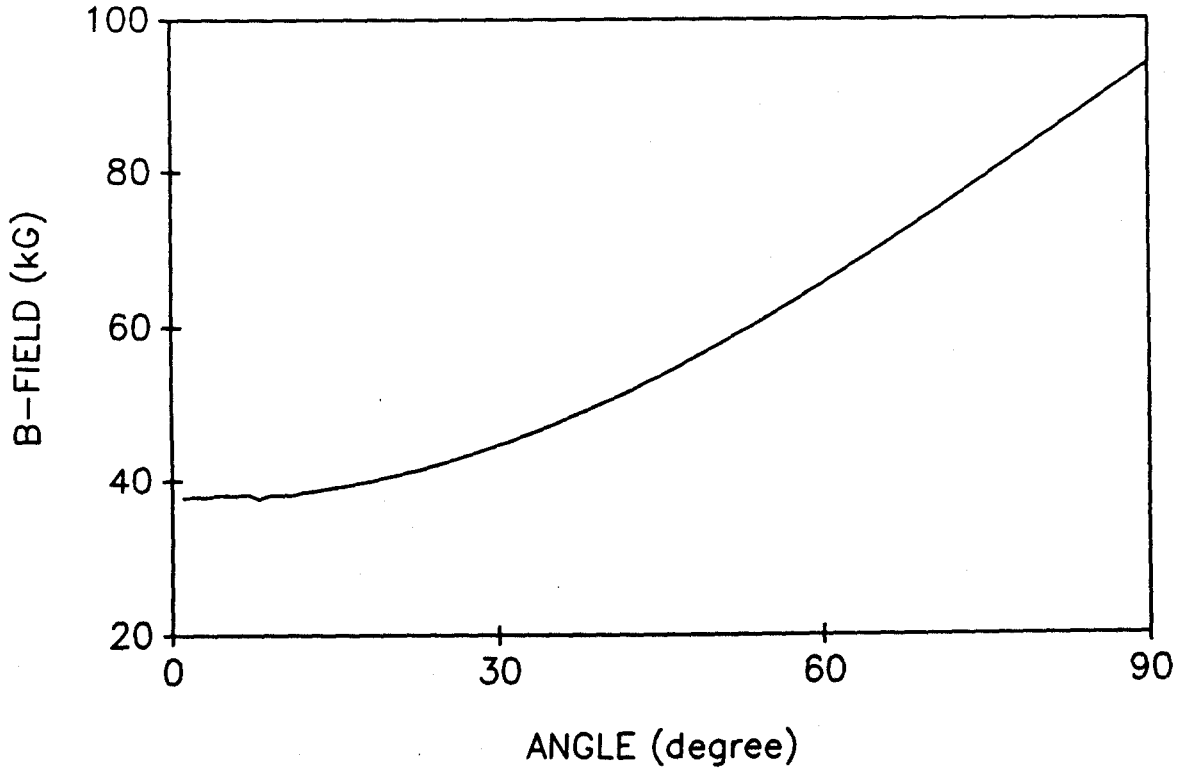
100
80
60
40
20
B-FIELD (kG)
0
30
60
90
ANGLE (degree)

Fig.6b